JOURNAL OF MATERIALS SCIENCE 29 (1994) 4778–4785

Crystallization behaviour of amorphous $Sc_{100-x}Fe_x$ alloys near $x=25$ composition

C. BANSAL, J.T.T. KUMARAN, G. RAJARAM
School of Physics, University of Hyderabad, Hyderabad 500 134, India

A detailed study of the process of crystallization in amorphous $Fe_{25}Sc_{75}$, $Fe_{28}Sc_{72}$ and $Fe_{25}Sc_{45}Zr_{30}$ alloys has been carried out using differential scanning calorimetry, X-ray diffraction and Mössbauer spectroscopic techniques. The complex multi-stage transformation process in $Fe_{25}Sc_{75}$ and $Fe_{28}Sc_{72}$ is understood in terms of polymorphous formation of an intermediate metastable crystalline phase of orthorhombic structure ($a = 0.521$ nm, $b = 0.648$ nm and $c = 1.212$ nm) and of likely Sc_3Fe stoichiometry, before final eutectic crystallization to stable Fe_2Sc and α-Sc.

1. Introduction

Preparation of amorphous $Fe_{100-x}Sc_x$ alloys near $x = 80$ and $x = 10$ which correspond to eutectic compositions in the phase diagram of Fe–Sc [1] have been previously reported [2, 3]. Zingg *et al.* [4] carried out resistivity, Hall effect and magnetic susceptibility measurements on $Fe_{90}Sc_{10}$, $Fe_{25}Sc_{75}$ and $Fe_{25}Sc_{37.5}Zr_{37.5}$ amorphous alloys. They compared the properties of the Fe–Sc system with those of Fe–Zr and found a difference in the behaviour of the two systems.

A measurement of the resistivity behaviour of $Fe_{25}Sc_{75}$ showed structural relaxation and a multi-staged crystallization process with changes in resistivity at five temperatures which also corresponded to peaks in the data from differential scanning calorimetry (DSC) [4]. Quadrupole splitting distributions evaluated from a Mössbauer spectroscopic study [3] showed an average quadrupole splitting of the same order as in the FeZr and NiZr systems. Both positive and negative electric field gradients (EFG) were found to be present. Recently Ryan *et al.* [5] have also reported a study of the magnetic properties of amorphous $Fe_{100-x}Sc_x$ alloys for $x = 9$, 10 and 11 compositions and find the magnetic behaviour of amorphous $Fe_{100-x}M_x$ (M = Sc, Y in group IIIb) distinct from that of $Fe_{100-x}M_x$ (M = Zr, Hf of group IVb).

In the present study we report a detailed DSC, X-ray diffraction and Mössbauer spectroscopic study of $Fe_{25}Sc_{75}$, $Fe_{28}Sc_{72}$ and $Fe_{25}Sc_{45}Zr_{30}$ amorphous alloys to understand the complex multi-staged transformation process occurring in these amorphous alloys.

2. Experimental procedure

Glassy ribbons of $Fe_{25}Sc_{75}$ were prepared by melt-spinning while $Fe_{28}Sc_{72}$ and $Fe_{25}Sc_{45}Zr_{30}$ were prepared by splat-cooling. Details regarding the preparation procedure can be found in Zingg *et al.* [4]. DSC studies were carried out on a DuPont 9900 computer thermal analyser at heating rates of 5, 20, 40 and 60 K min^{-1}. For X-ray diffraction and Mössbauer spectroscopy measurements the samples were heated to the temperature of DSC peaks at the same heating rate at which the peaks were observed. This ensured that the changes being observed in the X-ray and Mössbauer measurement corresponded to the transformations observed in DSC. Probability distributions for quadrupole splitting, $P(QS)$, were evaluated from the Mössbauer spectra. A linear correlation between isomer shift and quadrupole splitting was assumed [3] to fit the asymmetry in the intensities and widths of the Mössbauer lines.

3. Results

3.1. Differential scanning calorimetry

The DSC scans recorded at a heating rate of 40 K min^{-1} for $Fe_{25}Sc_{75}$, $Fe_{28}Sc_{72}$ and $Fe_{25}Sc_{45}Zr_{30}$ samples are shown in Fig. 1. There are four exothermal peaks (the last of which is beyond the measurement range in the 40 K min^{-1} scan but is visible in those at 5 and 20 K min^{-1}) for $Fe_{25}Sc_{75}$ as well as $Fe_{28}Sc_{72}$ alloys. For $Fe_{25}Sc_{45}Zr_{30}$ only two exothermic peaks are observed at all scan rates. For convenience of referring to the transformations corresponding to these peaks we label them in order of increasing temperature as A_1, A_2, A_3 and A_f for $Fe_{25}Sc_{75}$, B_1, B_2, B_3 and B_f, for $Fe_{28}Sc_{72}$ and C_1, C_2, C_f for $Fe_{25}Sc_{45}Zr_{30}$. The corresponding amorphous states are labelled as A_0, B_0 and C_0. Resistivity changes corresponding to these different transformations have been observed earlier (Fig. 2 of [4]).

There are two quantities of interest to be derived from DSC measurements: the activation energy (E) and the Johnson–Mehl–Avrami (JMA) exponent, which is related to the nature of the transformation.

0022–2461

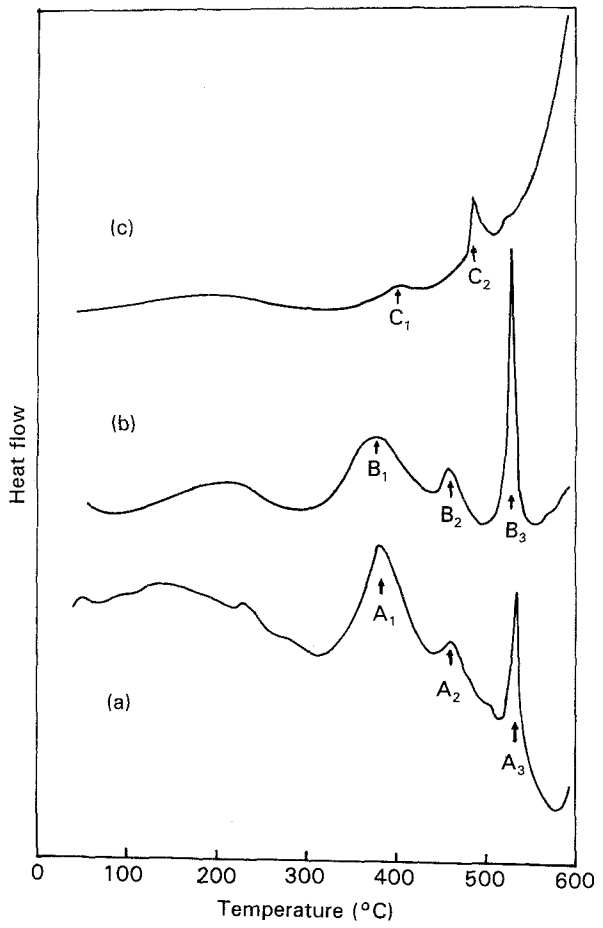

Figure 1 DSC scans for amorphous samples of (a) $Fe_{25}Sc_{75}$, (b) $Fe_{28}Sc_{72}$ and (c) $Fe_{25}Sc_{45}Zr_{30}$ recorded at a heating rate of 40 K min^{-1}. The transformation peaks are labelled for reference in subsequent analysis and discussion.

The activation energy is obtained from Kissinger's method [6] where an nth order reaction (solid → solid + gas) is assumed. For a constant heating rate ϕ this gives for the temperature of the DSC peak maximum (T_m) an expression

$$\ln\left(\frac{\phi}{T_m^2}\right) = \frac{-E}{RT_m} + \text{const.} \quad (1)$$

A plot of $\ln(\phi/T_m^2)$ against $1/T_m$ gives a straight line whose slope gives the activation energy E for the process.

However, to derive the JMA exponent one has to carry out a series of experiments at constant temperatures (isothermal scans) to get the fraction transformed (x) with time, at a given temperature. This is given by

$$x(t) = 1 - \exp[-k(t - t_0)^n] \quad (2)$$

where t_0 is the incubation time and n is the JMA exponent. This exponent is related to the crystallite nucleation and growth mechanisms. The activation energy is contained in the rate constant $k = k_0\exp(-E/RT)$. Both E and n can be determined by this procedure as outlined by Nazreth and Hadjipanayis [7]. In a multi-staged transformation process, it would be necessary to carry out isothermal scans at different temperatures and near each of the DSC peaks to get the fraction transformed before Equation 2 could be used.

However, it is also possible to get both n and E by an analysis of DSC scans at constant heating rates ϕ with fewer scans as has been suggested by Matusita *et al.* [8]. The JMA equation is generalized to a constant heating-rate process (in contrast to the usual JMA equation which is applicable to an isothermal process). Their analysis gives an equation

$$\ln[-\ln(1-x)] = n\ln\phi - 1.052\frac{mE}{RT} + \text{const.} \quad (3)$$

with $m < n < m + 1$. The parameter m depends on the dimensionality of growth ($m = 1, 2, 3$ for one-, and two- and three-dimensional growth). For growth alone (without nucleation) $n = m$ whereas if nucleation is also present $n > m$. A plot of $\ln[-\ln(1-x)]$ against $1/T$ at a given ϕ gives the slope $1.052\,mE/R$. From two such plots at different heating rates ϕ_1 and ϕ_2 one gets n as

$$n = \frac{1n[1n(1-x)_{\phi_1}/1n[1-x)_{\phi_2}]}{1n(\phi_2/\phi_1)} \quad (4)$$

The additional advantage of this method is that E can also be directly obtained from Kissinger plots, and from the value of $1.052\,mE/R$ derived above, m can be independently evaluated. Fig. 2 shows a plot of

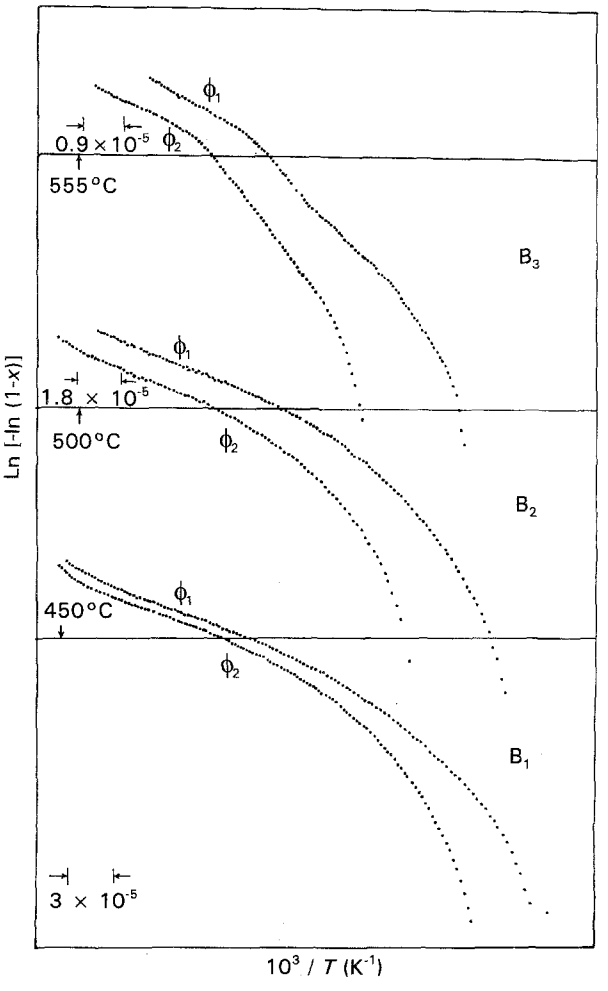

Figure 2 Plots of Equation 3 for a constant heating-rate process for amorphous $Fe_{28}Sc_{72}$ sample at heating rates of (ϕ_1) 20 K min^{-1} and (ϕ_2) 40 K min^{-1}.

$\ln[-\ln(1-x)]$ against $1/T$ for two heating rates (20 and 40 K min^{-1}) at the different DSC peaks. The fraction crystallized (x) was evaluated as a function of T by finding the area under the DSC peak from the starting temperature of the transformation to the temperature T. This was normalized to the total area under the full peak.

From Equation 3 we expect a set of parallel lines with intercepts governed by the heating rate ϕ and slopes given by $1.052\,mE/R$. However, we observe the lines to be parallel only during the later stages of transformation (higher temperatures). In the early stages also they are approximately parallel but the slope decreases in magnitude and finally approaches a fixed value. An explanation consistent with the data is a large value of activation energy during the early stages of the transformation as compared to the later stages. The activation energy obtained from the non-isothermal method is the activation energy for the whole crystallization process (E_c) and contains the activation energy for nucleation (E_n) as well as the activation energy for crystal growth (E_g) [9].

The activation energy for the crystallization process can also be independently obtained by the commonly used Kissinger method, which is a peak shift method. Fig. 3 shows Kissinger plots for the $Fe_{25}Sc_{75}$ sample and Table I shows the activation energy obtained from the slopes of these curves. The slopes of the non-isothermal plots, on the other hand, give a value for $1.052\,mE$. Table I also shows the values of mE obtained from the slopes of the non-isothermal curves in the higher temperature region and n as deduced from Equation 4. It is seen from this table that for all the peaks for $Fe_{25}Sc_{75}$ (A_1, A_2, A_3) and those of $Fe_{25}Sc_{45}Zr_{30}$ (C_1 and C_2), $n \simeq m$. This implies a growth-dominated process during the final stages of crystallization in these samples. The growth is one-dimensional for A_1, A_2, A_3 and C_1 whereas it is two-dimensional for C_2. During the early stages of the crystallization process the values of mE for the A_1, A_2 and A_3 peaks of $Fe_{25}Sc_{75}$ as obtained from the slopes of the curves at the low-temperature ends in Fig. 2 are 531, 1629 and 2263 kJ mol^{-1}, respectively. Assuming that the dimensionality of growth is the same during

TABLE I Crystallization characteristics and parameters from analysis of DSC data: activation energies (E) from Kissinger plots, mE and n as defined in Equations 3 and 4 for a constant heating process.

Sample	Peak	E (kJ mol^{-1})[a]	mE	n	Comments
$Fe_{25}Sc_{75}$	A_1	113	139	1.13	$n \simeq m$ (growth)
	A_2	274	334	0.92	$n \simeq m$ (growth)
	A_3	419	551	1.3	$n \simeq m$ (growth)
$Fe_{28}Sc_{72}$	B_1	202	199	0.92	$n \simeq m$ (growth)
	B_2	344	450	1.66	$n > m$ (nucleation and growth)
	B_3	516	529	2.03	$n \simeq m + 1$ (nucleation and growth)
$Fe_{25}Sc_{45}Zr_{30}$	C_1	315	398	1.3	$n \simeq m$ (growth)
	C_2	324	617	2.03	$n \simeq m$ (growth)

[a] Maximum error $\sim \pm 10\%$.

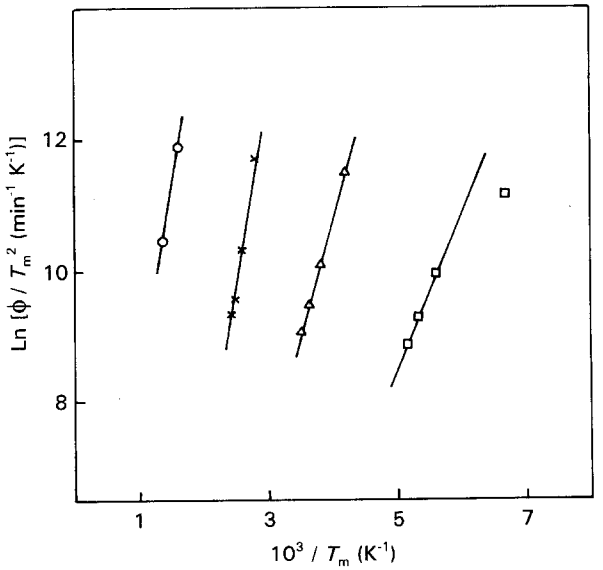

Figure 3 Kissinger peak-shift method plots for $Fe_{25}Sc_{75}$ sample to determine activation energies for the transformations occuring at (□) A_1, (△) A_2, (x) A_3 and (○) A_f. ϕ is the heating rate and T_m the peak temperature observed in DSC scans.

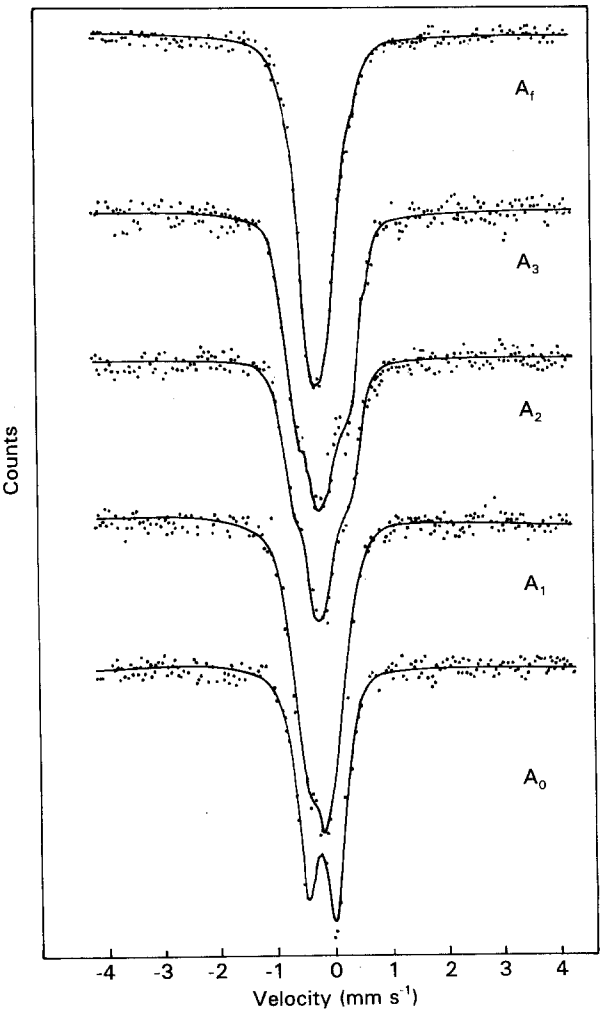

Figure 4 Mössbauer spectra recorded at room temperature after heating a-$Fe_{25}Sc_{75}$ sample to the DSC peak temperatures at the same heating rate at which peaks were observed in DSC scans (A_1, A_2, A_3). Spectra A_0 and A_f correspond to the amorphous state and final crystallized state, respectively.

the entire process, we use the value of m from Table I to get the activation energy (E_c) for the crystallization process from A_1, A_2 and A_3 as 430, 1336 and 1720 kJ mol^{-1}, respectively. This shows that the contribution to activation energy from the nucleation activation energy is large as compared to the growth activation energy. Large values of nucleation energy have also been observed in other systems and have been commented upon by Koster [10] but the reason for this is not yet understood.

3.2. Mössbauer spectroscopy and X-ray diffraction

Since the DSC peaks shift with heating rate, the samples were heated up to the peak temperatures at the same heating rate at which the peaks were observed in DSC scans, maintained there for 1 min and then cooled. Figs 4–6 show the Mössbauer spectra for $Fe_{25}Sc_{75}$, $Fe_{28}Sc_{72}$ and $Fe_{25}Zr_{30}Sc_{45}$, respectively. The spectra for the amorphous state (labelled A_0, B_0 and C_0) and for a final heat treatment at 600° C (A_f, B_f and C_f) are also shown in these figures. In the amorphous state the spectra are asymmetric but show well-defined quadrupole doublets. With each heat treatment the line shape changes, and the resolved doublet

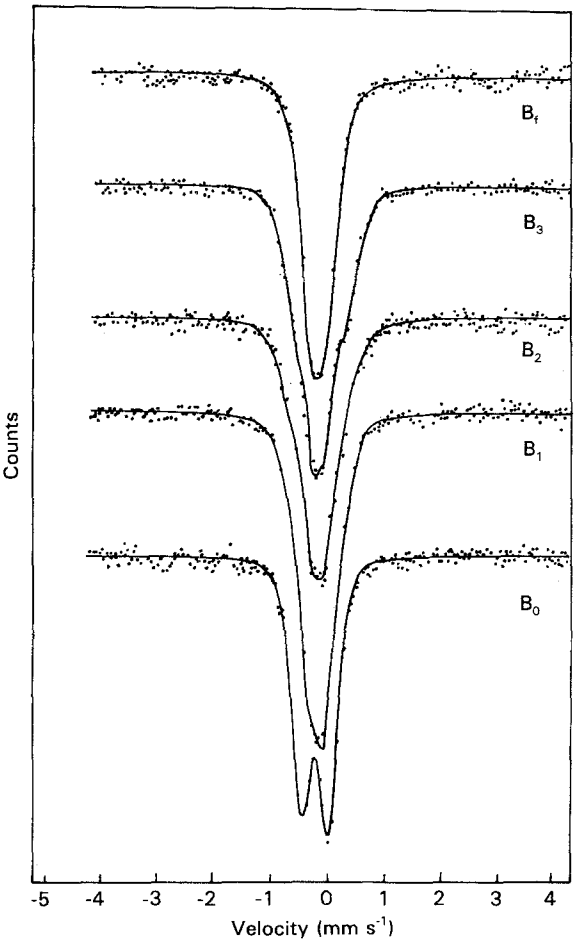

Figure 5 Room-temperature Mössbauer spectra for $Fe_{28}Sc_{72}$ sample after heating it to the DSC peak temperatures. B_1, B_2 and B_3 correspond to the intermediate transformation peaks observed in the sample.

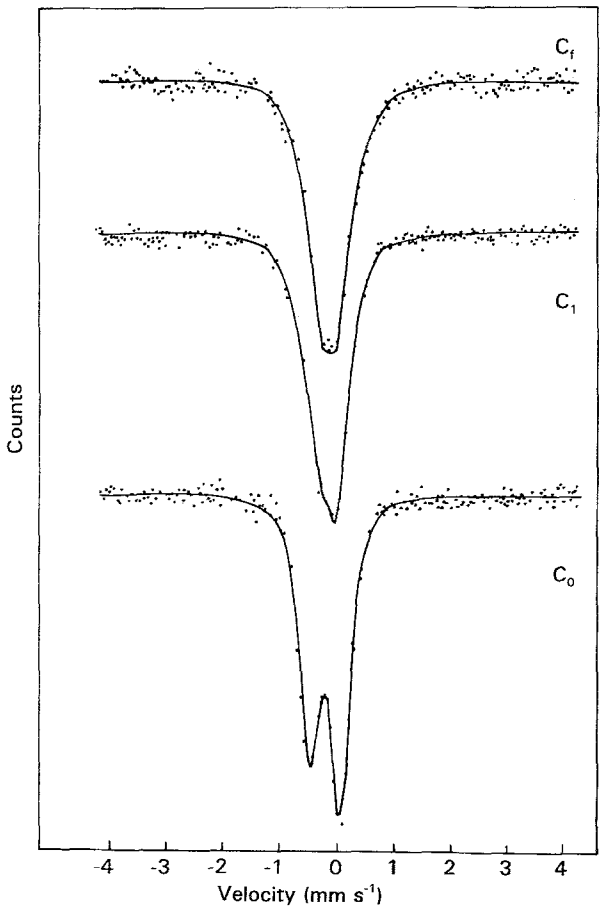

Figure 6 Mössbauer spectra for $Fe_{25}Zr_{30}Sc_{45}$ recorded after heating to DSC peak temperature C_1, for the amorphous state (C_0) and for the final crystallization product (C_f).

line shape seen in the amorphous state is no longer visible. These spectra were fitted to a quadrupole splitting distribution using Window's method [11]. A linear correlation of isomer shift with quadrupole splitting was assumed as taken previously by others [2, 3].

The quadrupole splitting distributions are shown in Figs 7–9. There is a noticeable change at each temperature of transformation. The average quadrupole splitting, $\langle QS \rangle$, at the peak positions in the distribution is shown in Table II. In the amorphous state of $Fe_{28}Sc_{72}$ there is a pronounced peak at $QS = 0.52$ mm s^{-1} and a very small shoulder at $QS \simeq 0.12$ mm s^{-1}. This suggests that there are two chemically different iron environments even in the amorphous state. For amorphous $Zr_{76}Fe_{26}$ also, the Mössbauer spectrum showed an asymmetric doublet structure [12] similar to our spectra and this was understood in terms of two different Fe environments. At the first transformation temperature the peak at $QS = 0.12$ mm s^{-1} becomes very prominant but there is also a large broadening of the distribution. At the next transformation temperature the distribution starts separating into two peaks, with the peak at the larger QS value occuring at ~ 0.9 mm s^{-1} which is more than the QS value of the main peak in the distribution for the amorphous state. Once again, this is quite similar to the behaviour of the amorphous Zr_3Fe system in which a metastable phase was detected in the early stages of crystallization. This metastable

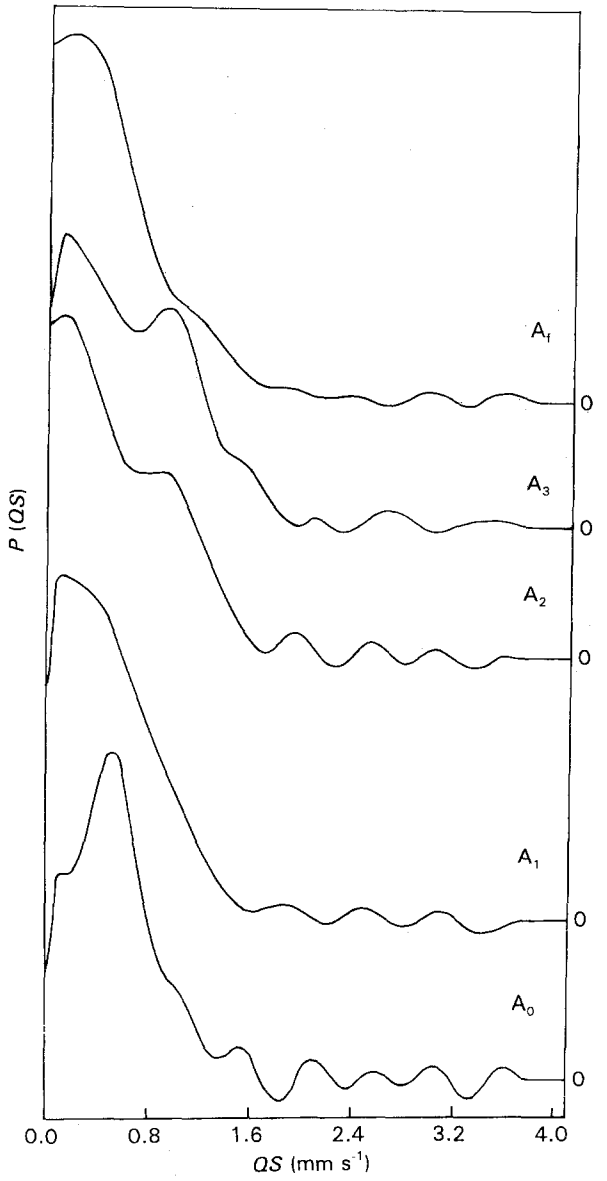

Figure 7 Quadrupole distributions evaluated for the Mössbauer spectra of $Fe_{25}Sc_{75}$ using Window's method. A linear correlation between isomer shift and quadrupole splitting was assumed. Plots are for A_0 (amorphous), A_1, A_2 and A_3 (intermediate stages) and A_f (final).

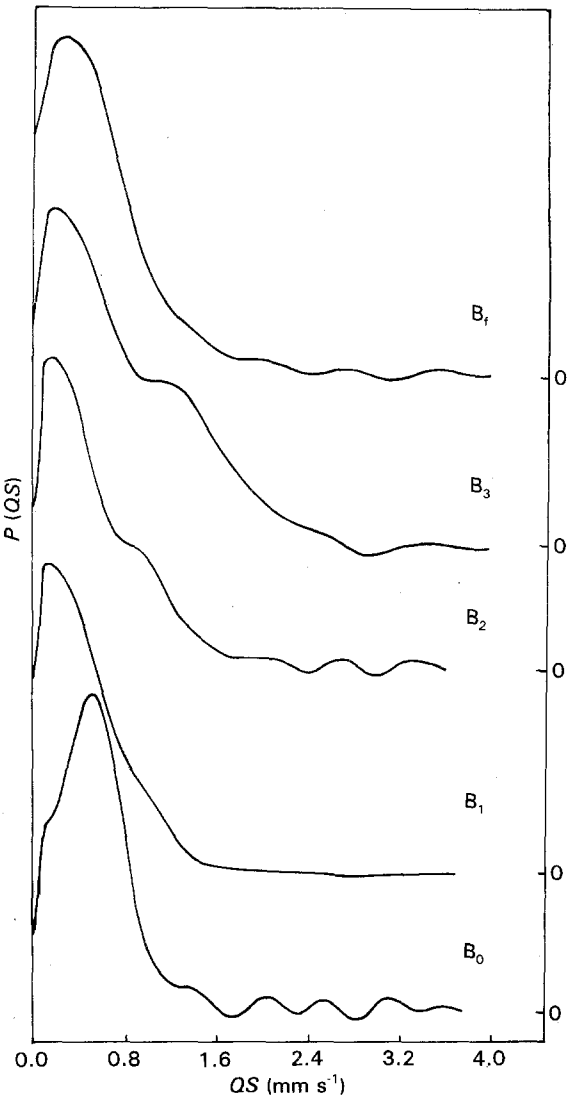

Figure 8 Quadrupole distributions corresponding to the various transformation stages B_0 (amorphous), B_1, B_2 and B_3 (intermediate temperatures corresponding to DSC peaks) and B_f (final crystallization) for amorphous $Fe_{28}Sc_{72}$.

state had a quadrupole splitting different from that of stable orthorhombic Zr_3Fe.

The second transformation process in $Fe_{25}Sc_{75}$ also suggests the formation of a metastable Sc_3Fe phase at this temperature. The two peaks separate out quite clearly in the next stage (A_3, B_3). This is confirmed very clearly in the X-ray diffraction patterns recorded after each transformation process (Figs 10–12). In the transformation stages at lower temperatures (A_1, A_2 and B_1) the X-ray patterns of $Fe_{25}Sc_{75}$ and $Fe_{28}Sc_{78}$ do not show any reflections either due to the amorphous phase or due to any crystalline phase. The crystallite size in these initial stages of transformation is probably too small to give any observable reflections. However, at the third transformation temperature (A_3) two small peaks appear in the diffraction pattern of $Fe_{25}Sc_{75}$ which are at positions ($d = 0.22951$ and 0.24140 nm) very distinct from those of peaks in the diffraction pattern for the final crystallized phase (A_f and B_f). Similarly B_2 also shows d values as seen in A_3.

The X-ray reflections from this metastable Sc_3Fe phase become more fully developed in the third stage (B_3) of transformation for $Fe_{28}Sc_{72}$ as compared to the third stage (A_3) of $Fe_{25}Sc_{75}$. From the X-ray reflections observed in B_3 the crystal structure of this metastable stage was determined. Table III shows the observed and calculated d values with an orthorhombic unit cell for parameters $a = 0.521$ nm, $b = 0.648$ nm, $c = 1.212$ nm. This metastable compound thus has a structure similar to Zr_3Fe which is also orthorhombic with $a = 0.3326$ nm, $b = 0.8807$ nm and $c = 1.0988$ nm. However, Mössbauer quadrupole splitting distributions corresponding to this transformation stage (A_3 and B_3) are similar and fully developed, indicating a better sensitivity of the Mössbauer probe for sensing the local environment even in very small crystallites.

For the final heat treatment at 600° C, the quadrupole distributions evaluated from the Mössbauer spectra show an average quadrupole splitting $\langle QS \rangle \simeq 0.23$

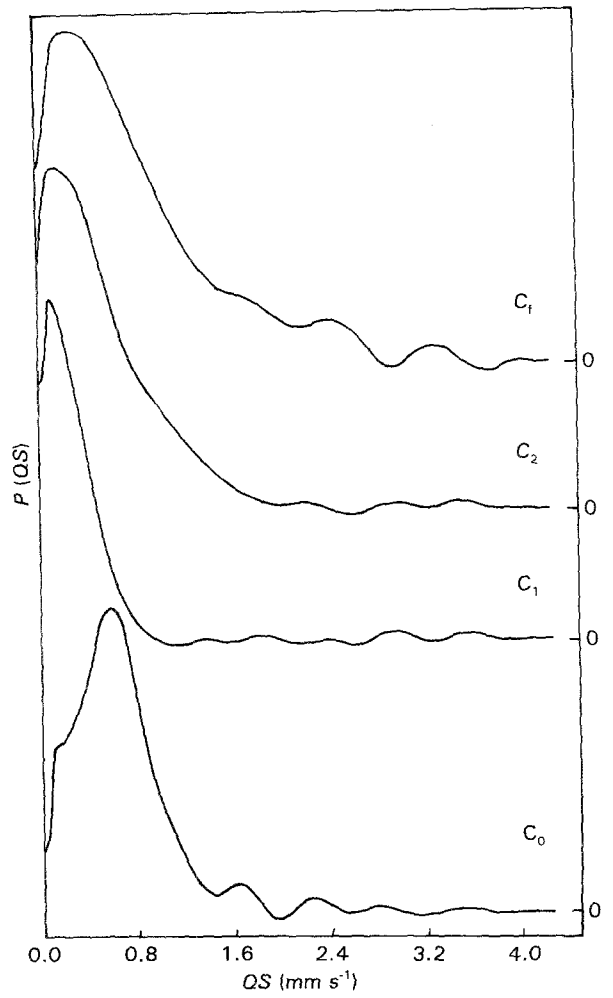

Figure 9 Quadrupole distributions for amorphous $Fe_{25}Sc_{45}Zr_{30}$ for the various transformation processes.

TABLE II Average quadrupole splittings, $\langle QS \rangle$, from probability distributions of the quadrupole splitting deduced from Mössbauer spectra at different transformation stages.

Sample	Peak	Heating temperature (°C)	$\langle QS \rangle$ (mm s^{-1})
$Fe_{25}Sc_{75}$	A_0	Amorphous	0.12, 0.52
	A_1	370	0.12, NR[a]
	A_2	450	0.09, 0.10
	A_3	520	0.09, 0.10
	A_f	600	0.23
$Fe_{28}Sc_{72}$	B_0	Amorphous	0.12, 0.52
	B_1	370	0.09, NR[a]
	B_2	450	0.12, 1.10
	B_3	520	0.17, 1.10
	B_f	600	0.28
$Fe_{25}Sc_{45}Zr_{30}$	C_0	Amorphous	0.57
	C_1	390	0.09
	C_2	480	0.14
	C_f	600	0.28

[a] Not resolved.

and 0.28 mm s^{-1}, respectively, for $Fe_{25}Sc_{75}$ and $Fe_{28}Sc_{72}$. These are in agreement with values reported earlier [3]. According to the phase diagram, the stable crystalline phases expected are α-Sc and Fe_2Sc. However, the Mössbauer spectrum for crystalline Fe_2Sc

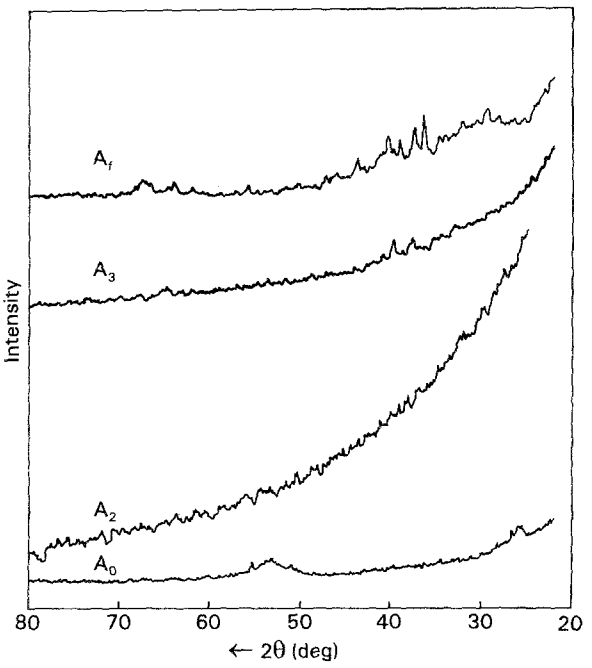

Figure 10 X-ray diffraction patterns for $Fe_{25}Sc_{75}$ recorded in the amorphous state (A_0), intermediate stages (A_2, A_3) and the final crystallization state (A_f).

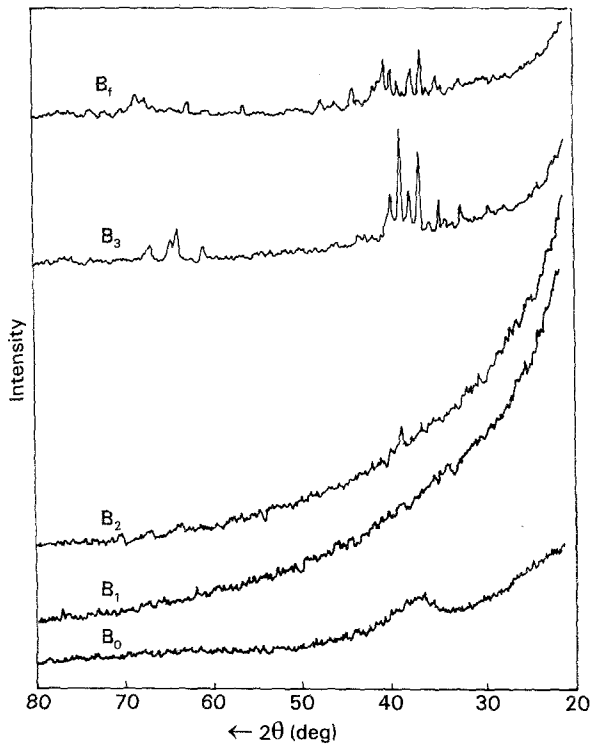

Figure 11 X-ray diffraction patterns for $Fe_{28}Sc_{72}$ recorded for the various transformation stages corresponding to the DSC peaks (B_1, B_2, B_3), in the amorphous state (B_0) and the final stage (B_f).

should consist of a hyperfine split pattern with two fields as reported by Smit and Buschow [13] for crystalline Fe_2Sc. This is different from the spectrum that is observed after crystallization of amorphous Fe–Sc (A_f in Fig. 4 and B_f in Fig. 5). The presence of a crystalline Fe_2Sc phase after the final heat treatment is not in doubt as shown by the X-ray diffraction patterns (A_f in Fig. 10 and B_f in Fig. 11). The prominent

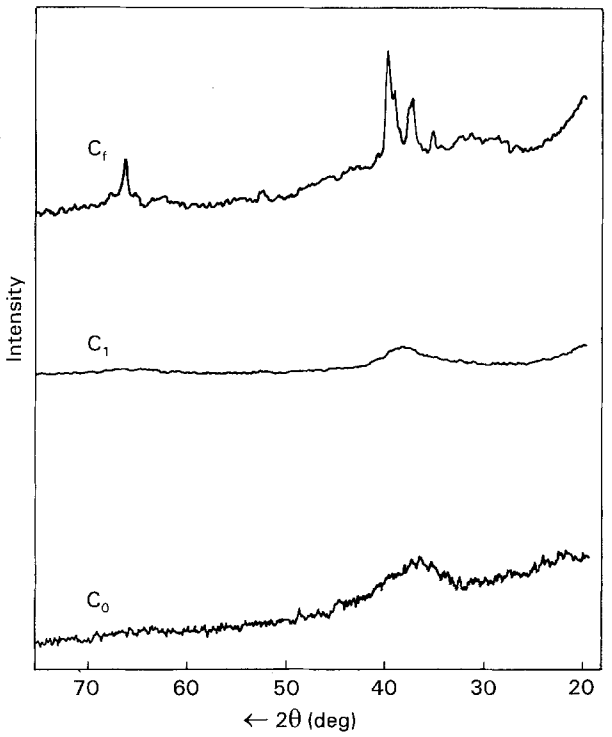

Figure 12 X-ray diffraction patterns for $Fe_{25}Sc_{45}Zr_{30}$ sample in the amorphous state (C_0), intermediate temperature heat-treatment (C_1) and final crystallization (C_f).

TABLE III Observed d values and those calculated with $a = 0.5212$ nm, $b = 0.6477$ nm, $c = 1.2123$ nm, for the metastable orthorhombic phase developed during polymorphous crystallization of a-$Fe_{28}Sc_{72}$.

d_{obs} (nm)	d_{calc} (nm)	$h\,k\,l$
0.2794	0.2792	1 2 0
0.2649	0.2656	1 0 4
0.2505	0.2509	2 0 2
0.2423	0.2425	0 0 5
0.2301	0.2297	1 2 3
0.2262	0.2271	0 1 5
0.2230	0.2219	1 0 5
0.1507	0.1505	1 4 2
0.1448	0.1450	1 4 3

lines of these diffraction patterns could be indexed to a hexagonal unit cell with parameters $a = 0.4983$ nm and $c = 1.6292$ nm as shown in Table IV. These lattice parameters are in good agreement with values reported [14] for Fe_2Sc ($a = 0.4972$ nm, $b = 1.628$ nm). The lattice parameters for this phase reported by Brand *et al.* [3] are $a = 0.49$ nm, $c = 0.78$ nm but we get a better agreement between observed and calculated d values for the lattice parameter values mentioned above.

The difference in Mössbauer spectra for stable crystalline Fe_2Sc obtained by arc melting and from crystallization of amorphous Fe–Sc could be due to the small size of Fe_2Sc crystals precipitated by the crystallization process. SEM micrographs taken after the crystallization (Fig. 13c) show isolated crystals of diameters about 3 μm only. The magnetic hyperfine

TABLE IV Observed and fitted d values for the Fe_2Sc phase with hexagonal unit cell of parameters $a = 0.4983$ nm and $c = 1.6292$ nm

d_{exp} (nm)	d_{calc} (nm)	$h\,k\,l$
0.2465	0.2468	1 1 1
0.2389	0.2382	1 1 2
0.2295	0.2298	0 1 6
0.2262	0.2264	1 1 3
0.2158	0.2158	0 2 0
0.2055	0.2048	0 1 7
0.1970	0.1979	1 1 5
0.1907	0.1907	0 2 4
0.1628	0.1629	0 0 10
0.1481	0.1481	0 0 11
0.1391	0.1390	0 3 3

field at room temperature can average to zero due to relaxation effects. The magnetic splitting can be seen only at low temperatures (see Fig. 2 of [3]).

The behaviour of the $Fe_{25}Sc_{45}Zr_{30}$ system seems to be intermediate between those of the $Fe_{25}Sc_{75}$ and $Fe_{25}Zr_{75}$ systems. The number of transformations is reduced to two, which is closer to the behaviour of

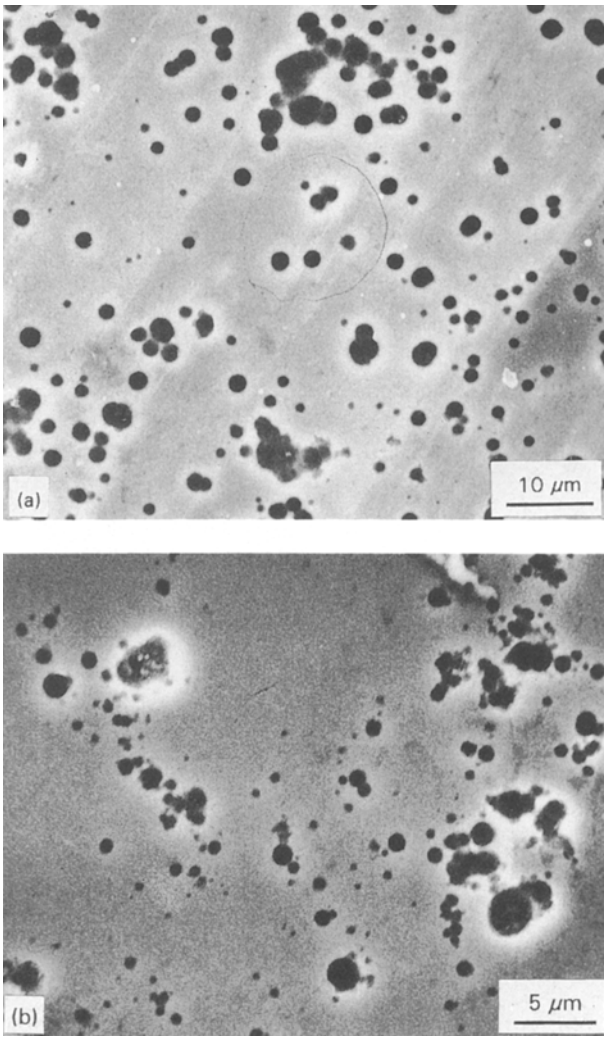

Figure 13 Scanning electron microscope pictures of (a) $Fe_{25}Sc_{75}$, (b) $Fe_{28}Sc_{72}$ and (c) $Fe_{25}Sc_{45}Zr_{30}$ samples after the final crystallization heat treatments (A_f, B_f, C_f). The diameter of the precipitated crystals is seen to be small ($\simeq 3$ μm).

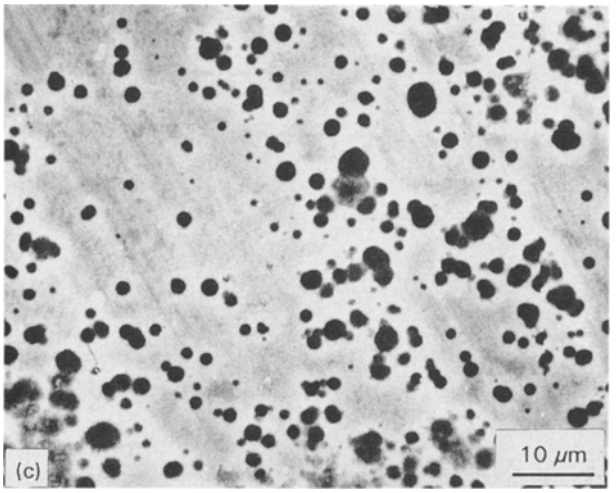

Figure 13(c) (continued).

$Fe_{25}Zr_{75}$. The quadrupole distribution in the second transformation stage (C_2) does not seem to separate out as clearly as in the case of $Fe_{25}Sc_{75}$. The X-ray reflections also do not correspond to the metastable Sc_3Fe phase. It is likely that at this stage a metastable FeScZr phase is formed, since both metastable Zr_3Fe and Sc_3Fe phases are possible. In resistivity and Hall effect measurements as well, $Fe_{25}(Zr_{1-x}Sc_x)_{75}$ alloys show a behaviour intermediate between those of $Fe_{25}Zr_{75}$ and $Fe_{25}Sc_{75}$ [4].

4. Conclusions

We have been able to follow the process of crystallization in the amorphous Fe–Sc alloy system through DSC, Mössbauer and X-ray diffraction studies carried out at various stages of the transformation. The transformation in this system proceeds by two crystallization reactions: polymorphous crystallization, followed by eutectic separation. The details of the different stages of transformation can be briefly summarized as follows:

1. In stage 1 there is a formation of small crystal lites which are undetected by X-ray diffraction but give a very large change in the quadrupole distributions of Mössbauer spectra.

2. In stages 2 and 3 a metastable phase of orthorhombic structure is formed as characterized by X-ray diffraction. In the Mössbauer quadrupole distributions this phase shows two distinct peaks separated from one another. This shows that Fe exists in two environments in this phase.

3. In the final stage stable crystalline Fe_2Sc precipitates of very small crystals are formed which do not give a saturated magnetic hyperfine field in Mössbauer spectra at room temperature.

4. The activation energy and dimensionality of growth for the different transformations stages were determined.

One final question that has to be addressed is regarding the physical process taking place between stage 2 and stage 3 of the transformation, which both correspond to formation of a metastable Sc_3Fe orthorhombic phase. Stage 3 of the transformation gives a distinct DSC peak as well as better separation between the peaks in the quadrupole distribution. One likely process that could be occuring at stage 3 is a disorder–order transformation of the metastable Sc_3Fe phase. This needs to be further investigated by more detailed experiments.

Acknowledgements

We are extremely grateful to Professor H.J. Güntherodt for his encouragement and support of this work. We thank Mr T. Richmond, Dr T. Zingg, Mr P. Reimann and Mr L. Rohr for preparation of samples used in this study. We thank Dr C.S. Sunandana for help with the DSC measurements.

References

1. E. A. BRANDES, (ed.), "Smithells Metals Reference Handbook" (Butterworths, 1983) pp. 11-256.
2. R. K. DAY, J. B. DUNLOP, C. P. FOLEY, M. GHAFARI and H. PASK, *Solid State Commun.* **56** (1985) 843.
3. R. A. BRAND, M.GHAFARI, W. KEUNE, H. J. GÜNTHERODT and H. W. GRONERT, *Z. Phys. Chem.* **157** (1988) 121.
4. T. ZINGG, T. RICHMOND, G. LEEMAN, H. JENNY, H. BRETSCHER and H. J. GÜNTHERODT, *Mater. Sci. Engng* **99** (1988) 179.
5. D. H. RYAN, J. O. STROM-OLSEN, W. B. MUIR, J. M. CADOGAN and J. M. D. COEY, *Phys. Rev. B* **40** (1989) 11208.
6. H. E. KISSINGER, *Anal. Chem.* **29** (1957) 1703.
7. A. NAZARETH and G. C. HADJIPANAYIS, *Phys. Rev. B.* **40** (1989) 5441.
8. K. MATUSITA, T. KOMATSU and R. YOKOTA, *J. Mater. Sci.* **19** (1984) 291.
9. S. MAHADEVAN, A. GIRIDHAR and A. K. SINGH, *Key Engng Mater.* **13–15** (1987) 359.
10. U. KOSTER, *ibid.* **13–15** (1987) 281.
11. B. WINDOW, *J. Phys. E* **4** (1971) 401.
12. I. VINCZE, F. van der WOUDE and M. G. SCOTT, *Solid State Commun.* **37** (1981) 567.
13. P. H. SMIT and K. H. J. BUSCHOW, *Phys. Rev. B* **21** (1980) 3839.
14. R. P. ELLIOT, in "Constitution of Binary Alloys" 1st Suppl. (*McGraw-Hill, New York*, 1965) *p.* 433.

Received 11 May 1993
and accepted 21 March 1994